DYNAMIC HYDRIDE PRECIPITATION DURING LOCA QUENCH PROCESS CAN SIGNIFICANTLY PRESERVE CLADDING'S DUCTILITY

H.G. SONNENBURG[1], F. BOLDT[1,2]

[1]*Gesellschaft für Anlagen- und Reaktorsicherheit (GRS) gGmbH*
Boltzmannstr. 14, 85748 Garching, Germany
[2]*Department of Nuclear Technology, Technical University of Munich*
Boltzmannstr. 15, 85748 Garching, Germany

ABSTRACT

During a LOCA transient, the cladding of a fuel rod may undergo ballooning burst, oxidation and short-term secondary hydriding of the cladding which cladding's ductility, thus fuel rod rupture could occur if the mechanical load from a thermal shock during a quench process exceeds the burst stress level.

Recent German regulatory rulemaking sets new limits for oxidation and hydrogen uptake during LOCA. The oxidation parameter ECR (equivalent cladding reacted) was limited to 17% in the past. Nowadays, this ECR limit is depending on cladding's hydrogen content, thus it's reduced to smaller values below 17% if hydrogen uptake increases. The dependency between ECR limit and hydrogen content was shown by experimental ring compression tests. However, integral LOCA tests in Japan reveal that this relationship might be very conservative when checked against these LOCA test results. The discrepancy could be largely explained if the dynamics of hydrogen precipitation and hydride formation during quenching are taken into account.

1 Introduction

Zircaloy fuel rod cladding used in light water reactors is susceptible for hydrogen (H) uptake and cladding oxidation, which is a normal process during reactor operation. The hydrogen content during normal operation reaches values up to a few hundred parts per million (ppm), dependent on the cladding material. Within a loss-of-coolant accident (LOCA), the fuel rod temperature and inner pressure increase which causes cladding ballooning and eventually burst of fuel rods. The cladding's inner side near the burst opening will face the so-called secondary hydriding. The following quenching-induced thermal shock loads the cladding under precipitating hydrides which progressively reduces cladding's ductility.

The Integral Thermal Shock (ITS) tests in Japan showed LOCA-typical temperature transients on claddings at various hydride contents and oxidation levels[1],[2]. Some tested fuel rods, although showing precipitated hydride content above 3000 ppm H at the end of transient, remained intact. These test results contrast with nil-ductility limits which have been derived from Argonne National Lab (ANL) ring compression tests[3]. Nil-ductility depends on both oxidation level and hydride content. It is suspected that the hydride content at the end of temperature transient is not representative for the assessment of cladding's ductility.

This work focuses on the hydride precipitation dynamic occurring during LOCA transient which may explain the significant preservation of cladding's ductility during the critical quench loading phase.

2 Cladding rupture and ECR-criterion

In a LOCA transient the cladding of a fuel rod may balloon, oxidize and burst. After fuel rod burst, the inner cladding surface is exposed to steam and oxidizes additionally. This inner oxidation provokes a large amount of hydrogen uptake in short distance to the burst opening reaching values of about 3000 to 4000 ppm H. Therefore, the vicinity of the burst opening experiences a detrimental combination of high oxygen uptake and hydrogen uptake. Both uptakes significantly affect cladding's ductility.

Previously, the zero ductility was expected to occur due to cladding oxidation only. Regulatory limits therefore allowed a maximum cladding consumption of the metallic cladding thickness due to oxidation (ECR: equivalent cladding reacted) of 17 %[4]. This ECR value was set constant regardless of the cladding's hydrogen content. Because the operation of fuel rods at high burnup led to significant hydrogen uptake in the cladding, it became obvious this may also affect cladding's ductility. This motivated ANL to investigate the ECR limit and its dependence on hydrogen uptake.

ANL accomplished ring compression tests (RCT) which provide a huge data base for the determination of the cladding ductility. Herb[3] analysed these ANL RCTs with FEM technique and found a dependence of the burst stress on both oxidation and hydrogen uptake. This dependence is expressed as burst stress σ_{burst} to yield stress σ_{yield} ratio R as function of ECR and hydride content $\mathrm{c(H)}$.

$$R = \frac{\sigma_{\mathrm{burst}}}{\sigma_{\mathrm{yield}}} = a_0 + \left(a_{\mathrm{ECR}} + a_{\mathrm{H,ECR}} c(H)\right) ECR + a_{\mathrm{T}} T + a_{\mathrm{H}} c(H) \qquad (1)$$

with regression coefficients as listed in table 1. The equation (1) is of generic applicability as far as the same shape of hydride precipitates is given as observed in ANL RCTs.

Table 1: Regression coefficients in equation (1) for various cladding materials from Herb[3]

Regression Coefficients	Value
a_0	1.62
$a_{\mathrm{T}} \quad (\frac{1}{^{\circ}C})$	$1.8 \cdot 10^{-3}$
$a_{\mathrm{ECR}} \quad (\frac{1}{\%\,\mathrm{ECR}})$ (Zry-4, ZIRLO)	$-4.2 \cdot 10^{-2}$
$a_{\mathrm{ECR}} \quad (\frac{1}{\%\,\mathrm{ECR}})$ (M5)	$-3.7 \cdot 10^{-2}$
$a_{\mathrm{H}} \quad (\frac{1}{\mathrm{ppm\,H}})$	$-1.05 \cdot 10^{-4}$
$a_{\mathrm{H,ECR}} \quad (\frac{1}{\%\,\mathrm{ECR}\ \ \mathrm{ppm\,H}})$	$-1.08 \cdot 10^{-4}$

Of particular interest is the ratio $R = 1$. It describes nil-ductility, the transition from ductile to brittle cladding behaviour. At $R = 1$ the burst stress is identical to the yield stress, the associated temperature is the nil-ductility temperature (NDT) or ductile-brittle transition temperature (DBTT). This NDT will be taken later in order to assess cladding's ductility during the thermal shock at fuel rod quench.

Setting both $R = 1$ and $T = 135\,^{\circ}\mathrm{C}$ in Equation (1) provides the limiting relation for the oxidation level (ECR limit) as function of hydrogen content $c(H)$. This criterion should be applied in safety demonstration for LOCA transients in Germany. The safety margin of this criterion will be discussed later.

Major problem in applying this ECR limit is the prediction of the hydride uptake due to secondary hydriding. KIT LOCA quench tests as well Japanese ITS tests reveal huge scattering for secondary hydriding after burst of cladding (see upper and lower bounding curve for scattering data in figure 1)[5].

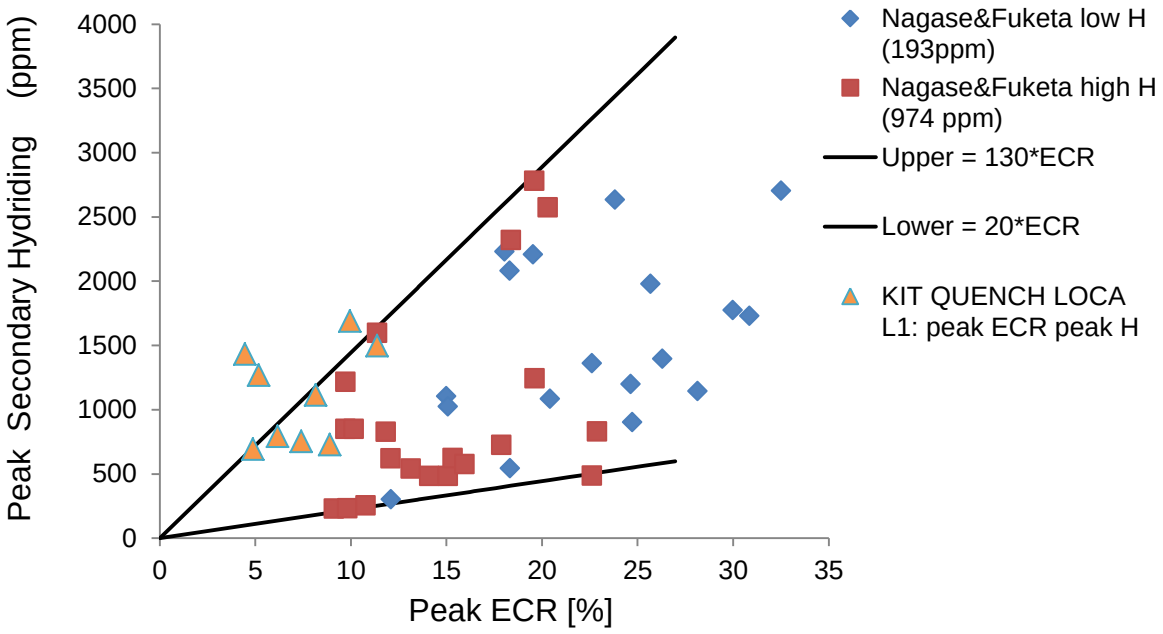

Fig. 1**:** Japanese ITS tests for low and high secondary hydriding compared with KIT-QUENCH-tests

Therefore, recent licencing approach followed at U.S.NRC restricts the hydrogen uptake to the operational hydrogen uptake only and ignores the secondary hydriding within their ECR limiting criterion[6]. This approach has been justified on basis of additional 4-point bending tests on ballooned and burst claddings showing significant fracture toughness.

Also the more realistic Japanese ITS test data measured by Nagase and Fuketa[2] reveal significant safety margin with respect to the high level of hydride content observed at end of test. The limiting ECR curve (green line in fig. 2), deduced from equation (1) at $R = 1$ and $T = 100\,°C$, is in far distance to the measured failure/none-failure threshold data by Nagase and Fuketa when post-test hydride content is regarded. After secondary hydriding the red curve in figure 2 have to be shifted to higher hydride contents for post-test condition.

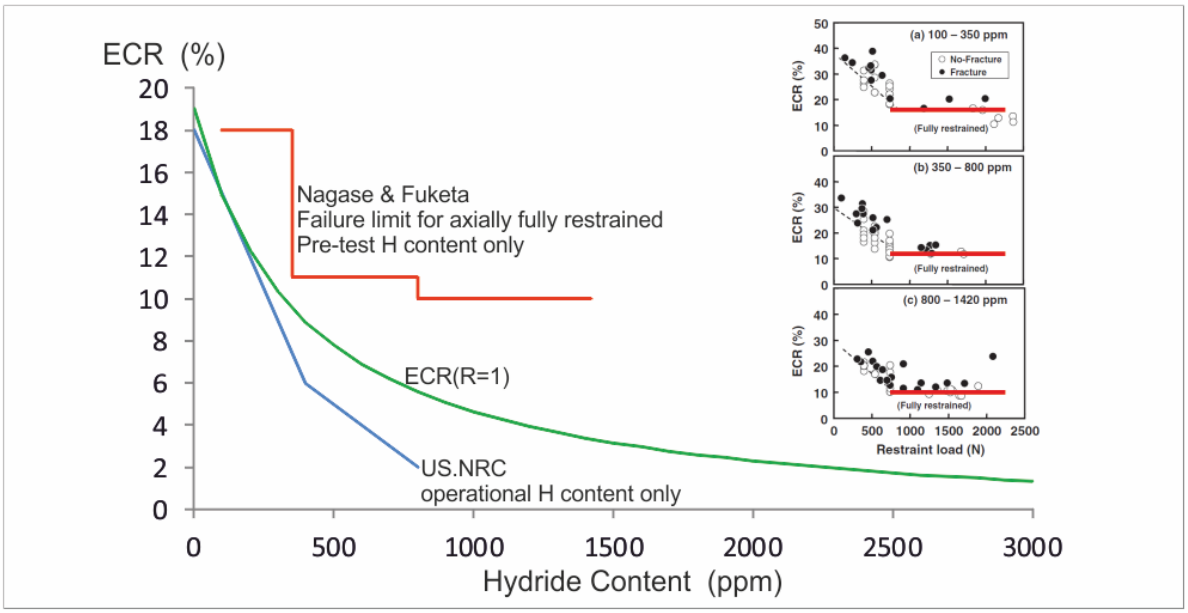

Fig. 2: Comparison of ECR limit (at T=100 °C, R=1) with U.S.NRC limit and failure limits of Nagase and Fuketa (at T=100 °C)

To explain the real impact of secondary hydriding on ductility, there must be another phenomenon involved in LOCA testing which can provide significant safety margin relative to the ECR(R=1)criterion. It is hypothesized that delayed hydrogen precipitation could lead to effective hydride contents which are far below the fully precipitated values at the end of transient.

3 Delayed precipitation of hydrides

Lacroix et al. published recently measured ANL tests on cyclic hydride dissolution and precipitation[7]. In this work x-ray diffraction (XRD) is used to measure the dynamics of dissolution and precipitation of hydrides in-situ. This measuring technique instantaneously follows the quantity of precipitated hydrides with high precision. The accuracy is about $\pm$5 ppm hydride content combined with $\pm$3 °C temperature variation[1].

In previous experimental investigations the precipitation and dissolution of hydrides had been determined with various measurement techniques for different materials in different temperature ranges[8],[9],[10],[11]. These measurements exhibit some large deviations between each other. To the authors knowledge only ANL's XRD measurements as in[7],[8] provide a reasonable high time resolution to apply this to a LOCA time scale. Therefore, we followed our own modelling approach based on XRD data.

Generally, the concentration for the terminal solid solubility for dissolution C_{TSSd} and precipitation C_{TSSp} can be expressed as exponential correlation with

$$C_{\mathrm{TSSd}} = A_1 \exp\left(-\frac{B_1}{\mathrm{T}}\right) \tag{2}$$

and

$$C_{\mathrm{TSSp}} = A_2 \exp\left(-\frac{B_2}{\mathrm{T}}\right). \tag{3}$$

Starting with known exponential correlations we found that modified parameters for A_1, A_2, B_1 and B_2 correlate XRD measured precipitation of hydrogen and dissolution of hydrides best with values in Tab. 2.

Tab. 2: Correlation coefficients for TSSd and TSSp data

Coefficient	Value
A_1	$1.75 \cdot 10^6$ppm
B_1	6060 K
A_2	$1.665 \cdot 10^5$ ppm
B_2	4145.72 K

Deviation of dissolved hydrogen content from C_{TSSd} provokes a dissolution/precipitation rate with rate constants which have been determined from XRD test results. We found:

$$\frac{\mathrm{d}C_{\mathrm{diss}}}{\mathrm{dt}} = 10^{-4}\frac{1}{s}\cdot\left(C_{\mathrm{TSSd}} - C_{\mathrm{diss}}\right) \qquad if \quad C_{\mathrm{TSSp}} > C_{\mathrm{diss}} > C_{\mathrm{TSSd}} \tag{4}$$

$$\frac{\mathrm{d}C_{\mathrm{diss}}}{\mathrm{dt}} = 0.5\frac{1}{s}\cdot\left(C_{\mathrm{TSSd}} - C_{\mathrm{diss}}\right) \qquad if \quad C_{\mathrm{diss}} < C_{\mathrm{TSSd}} \tag{5}$$

$$\frac{\mathrm{d}C_{\mathrm{diss}}}{\mathrm{dt}} = \alpha^2\cdot\left(C_{\mathrm{TSSp}} - C_{\mathrm{diss}}\right) + 10^{-4}\frac{1}{s}\cdot\left(C_{\mathrm{TSSd}} - C_{\mathrm{diss}}\right) \qquad if \quad C_{\mathrm{TSSp}} < C_{\mathrm{diss}} \tag{6}$$

The dissolution rate parameter α^2 follows an exponential temperature relation with:

[1] Depending on thermo-couple precision, values based on private communication

$$\alpha^2 = 2 \cdot 10^5 \frac{1}{s} \exp\left(-\frac{10^5 K}{\mathrm{T}}\right) \qquad (7)$$

But α^2 can vary within $0.01\frac{1}{s}$ and $0.1\frac{1}{s}$ only. This parameter follows the exponential relation as long as the temperature rises. If temperature falls, the α^2 value remains constant on the level reached.

Physical interpretation is that protons progressively migrate towards precipitated hydrides with rising temperatures. But if temperature cools down, the location of protons already reached is close to the precipitated hydrides thus diffusion distance remains shorter and precipitation is more effective which justifies α^2 values above those from exponential relation (7).

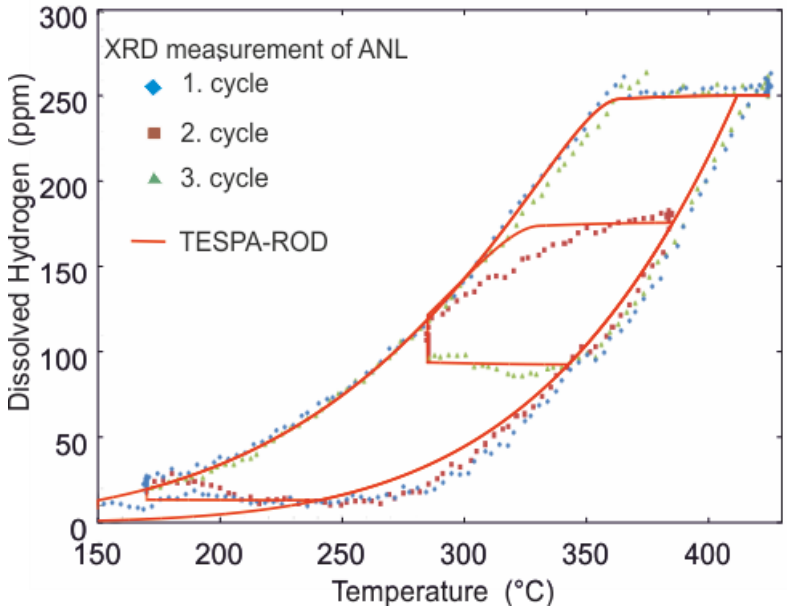

Fig. 3: Comparison of TESPA-ROD calculation results and the XRD measurements of ANL thermal cycling tests[7]

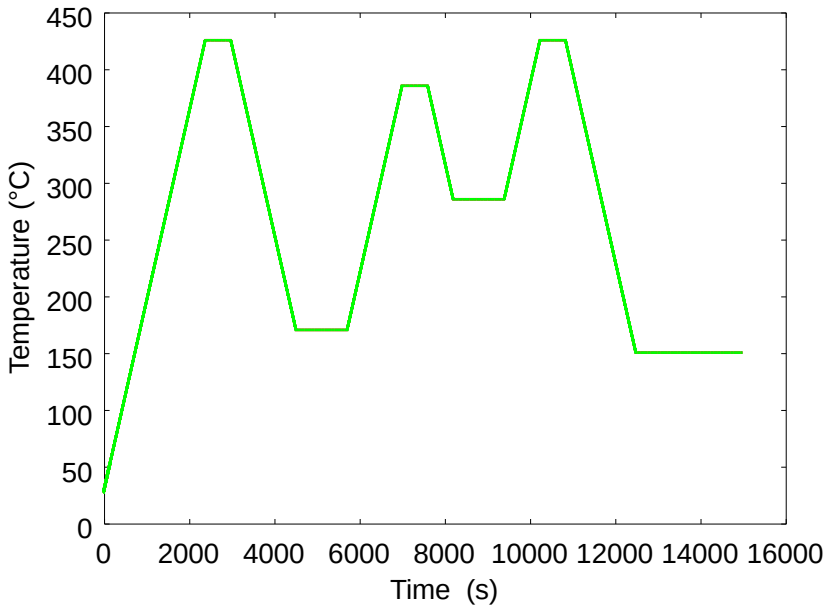

Fig. 4: Temperature profile of ANL cycling tests used for TESPA-ROD calculation[7]

The precipitation/dissolution model above (equation 2 through 7) has been implemented in the GRS fuel rod code TESPA-ROD. The quality of model verification is shown in figure 3 comparing the separate effect test data of XRD measurements[7] with our code prediction.

The test comprises three thermal cycles, which are shown in figure 4. It begins with a rise in temperature from room temperature up to 425 °C (cycle 1) where all hydrides are dissolved. The first cooldown from 425 °C to 175 °C shows precipitation close to a metastable TSSp curve. In cycle 2 the temperature rises to 385 °C only. The subsequent second cooldown from 385 °C to 285 °C shows again hydride precipitation which follows the previous TSSp curve. When temperature development stops at 285 °C for about 1200 s, further hydride precipitation takes place (see vertical line at 285 °C in Fig. 3). At this point one can understand that TSSp is metastable only and continued precipitation would finally approach the TSSd curve if sufficient time beyond 1200 s would be provided.

As can be seen, the TESPA-ROD model for hydride precipitation described above provides a very close prediction for all three temperature cycles. This model successfully reproduces the metastable TSSp curve as well as it predicts the precipitation during constant temperature hold period which would finally give an asymptotic approach to the stable TSSd curve. The TESPA-ROD model also reproduces the TSSd curve when temperature starts rising. Thus, this model reproduces the measured dynamics of dissolution/precipitation correctly including its hysteresis for cycling temperatures.

Because the XRD measurements during cooldown have been reproduced with the TESPA-ROD model as well, we generally expect dependable predictions even for faster cooldown transients like those of a LOCA quench transient because proton diffusion in Zircaloy limits the growth rate of precipitating hydrides and non-linearity in the driving force ($C_{\mathrm{TSSp}} - C_{\mathrm{diss}}$) for this diffusion is not to be expected.

The orientation of precipitated hydrides has a large influence on cladding's ductility. TESPA-ROD differentiates between radial and azimuthal oriented hydrides depending on the stress state and temperature gradient across the cladding thickness, depending on measurements of Cinbiz[12].

4 TESPA-ROD prediction for LOCA test transients

The GRS fuel rod code TESPA-ROD predicts the fuel rod behaviour for both RIA and LOCA transients, and recently was extended for long-term storage transients. The German technical inspection agency utilizes the TESPA-ROD code for regulatory safety assessments on core loading schemes before start of a new reactor cycle. This kind of safety assessment is focused on the determination of the number of fuel rods which might burst under LOCA transient condition. Therefore, the code predicts for each fuel rod in a loading scheme the oxidation, ballooning, burst/none-burst behaviour and secondary hydriding. The code quantifies for each fuel rod the oxidation (measured as ECR) and the quantity of hydrogen uptake due to secondary hydriding if burst of cladding has been detected.

During the LOCA transient, α-phase -Zircaloy transforms to β-phase Zircaloy at high temperatures. The following cooldown is accompanied by a retransformation to the α-phase, which is often described as prior-β-phase. TESPA-ROD code considers the dynamic α-β-phase transformation of Zircaloy based upon the modelling of Foregon et al.[13] Within this dynamic phase transition model, phase boundaries (β to α-β and α-β to α) depend on both the oxygen content and hydrogen content, thus both cladding oxidation and secondary hydriding have influence on these boundaries. It is important to note, that the hydride precipitation model described above is applicable to α-phase-Zircaloy only.

Cladding's oxidation, measured in ECR and weight gain τ, is quantified from oxidation correlations (e.g. Baker&Just[14] or Cathcart&Pawel[15]) available in the code. Secondary hydriding

is quantified based on a model prediction which relates this hydrogen uptake to the oxidation rate.

While the quantification of ECR involves low uncertainty, the TESPA-ROD model for hydrogen uptake has large. This large uncertainty is a consequence of scattering H uptake data which show a weak correlation between oxidation and H uptake only.

The model for H uptake $\dot{\eta}$ applied in TESPA-ROD is:

$$\dot{\eta}\,\frac{\text{wppm H}}{\text{s}} = \dot{\tau}\,(1+\varepsilon)\begin{cases} 5400\ \frac{\text{wppm H}}{\frac{\text{kg O}}{\text{m}^2}} & \text{if } T < 1000^\circ\ C \\ 5400 \ldots 1810\ \frac{\text{wppm H}}{\frac{\text{kg O}}{\text{m}^2}} & \text{if } 1000^\circ\ C < T < 1200^\circ\ C \\ 1810\ \frac{\text{wppm H}}{\frac{\text{kg O}}{\text{m}^2}} & \text{if } T > 1200^\circ\ C \end{cases} \tag{8}$$

Where $\dot{\tau}$ is the oxygen uptake rate ($\frac{\text{kg O}}{\text{m}^2\cdot\text{s}}$) and ε the circumferential cladding expansion[16]. Because of the huge uncertainties in H uptake, TESPA-ROD follows the upper bounding values for H uptake (compare Fig. 1, equation (8)).

The ratio of burst stress to yield stress (equation (1)) derived from RCTs can be recast for the NDT, which is given if the ratio of stresses approaches unity. That is, cladding's stress/strain relation has no plastic part beyond the yield stress. With $R = 1$ the NDT is now depending on ECR and hydrogen uptake $c(\text{H})$:

$$\text{NDT} = \frac{1}{a_\text{T}}\Big[1 - a_0 - \Big(a_\text{ECR} + a_\text{H,ECR}\,c(\text{H})\Big)\,\text{ECR} - a_\text{H}\,c(\text{H})\Big]. \tag{9}$$

While material properties like Young's modulus or thermal expansion instantaneously follow fast changes of temperature, the growth of precipitating hydrides follows the change in temperature with significant time delay. Due to this difference over time it is suspected that NDT occurs after the maximum load of the quenching process is already gone. Or in other words, at the time of maximum quench load the ductility is largely preserved although large hydrogen content from secondary hydriding might exist in the cladding because precipitation and thereof nil-ductility occurs later in time.

The timing of maximum quench load can be taken from the temperature gradient which develops during cooldown across the cladding thickness. Cladding stress during steep cooldown can be estimated from this temperature difference. The steeper the temperature gradient, the larger the circumferential stress in the outer cladding is. Subsequent graph illustrates the stress distribution across the cladding (Fig. 5).

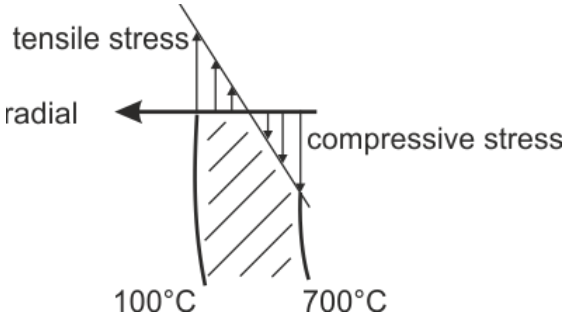

Fig. 5: Schematic circumferential stress distribution over the cladding thickness during quenching process

The circumferential stress $\sigma_{\Theta\Theta}$ occurring at the cladding surface due to rapid cooldown can be expressed with:

$$\sigma_{\Theta\Theta} = \frac{\alpha\, E\, \Delta T}{2(1-\nu)} \left[\frac{1}{\ln\left(\frac{d_o}{d_i}\right)} - \frac{2}{\left(\frac{d_o}{d_i}\right)^2 - 1} \right]. \qquad (10)$$

Here, α is the thermal expansion coefficient, E is Young's modulus, ν is Poisson ratio, d_i and d_o are inner and outer diameter, respectively. ΔT is the temperature difference across the cladding thickness (e.g. ΔT=700 °C - 100 °C).

The time development of the quench load (10) in comparison to the time development of the nil-ductility temperature (9) provides the required insight into that hydride quantity which is relevant for the detrimental effect. These time developments can be investigated when looking on integral LOCA tests (ITS tests) performed by Nagase and Fuketa[2].

5 Simulation of ITS tests of Nagase and Fuketa

Nagase and Fuketa heated a single fuel rod in an oven up to 1200 °C. This temperature is kept constant as long as the oxidation reaches predetermined oxidation levels, measured in ECR-% (Fig. 7). The cladding balloons and burst during oxidation. When the predetermined oxidation is reached the oven is shut down and the fuel rod cools down to about 700 °C. Then the fuel rod is submerged into boiling water (at T=100 °C) which provides a fast cooldown. The fast cooldown (quenching) shows a temperature drop with 600 K within about 3 seconds (200 K/s) or even faster. Depending on the oxidation level and hydrogen uptake, this kind of thermal shock has the potential to break the cladding if cladding's ductility is insufficient.

These ITS tests are non-standard LOCA tests, because during fast cooldown the cladding is axially restrained by partial or full prevention of axial contraction of cladding which would follow the cooldown of the cladding[2]. Axial forces up to 2500 N are measured under fully constrained condition, that is, the contraction of the cladding due to cooldown is totally prevented. This testing procedure leads to high additional stresses during quenching and therefore allows identifying cladding failure limits related to oxidation and hydrogen content (see dashed line in Fig. 6). This kind of axial load artificially penalizes the cladding failure threshold beyond realistic LOCA condition.

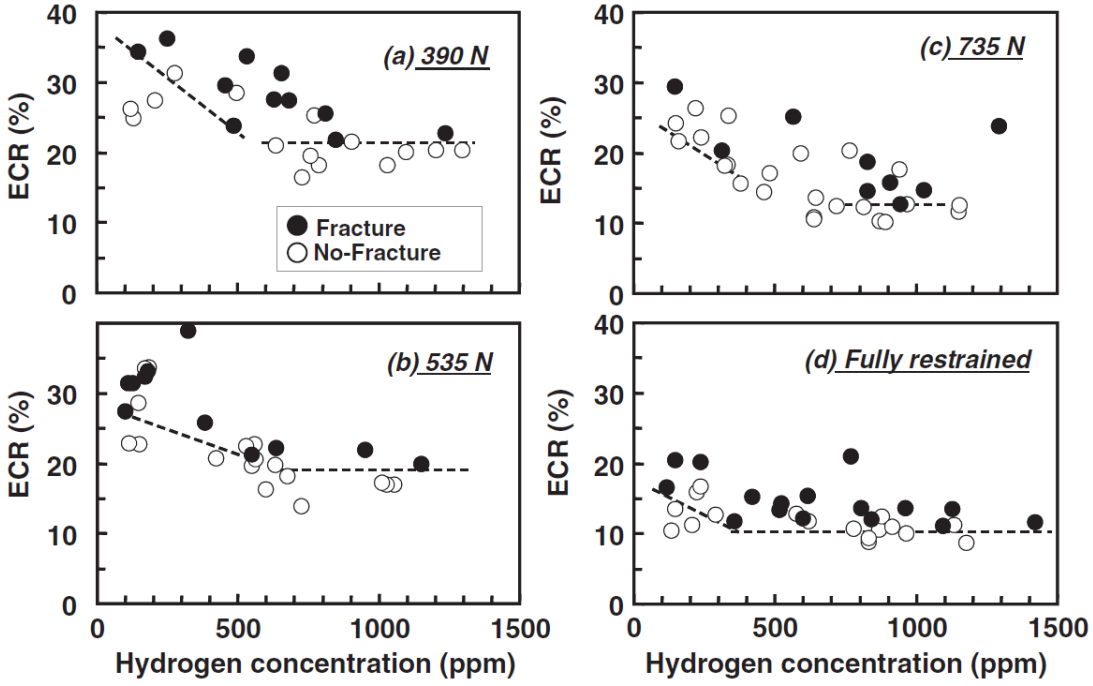

Fig. 6: Failure map taken from Nagase and Fuketa[2] for varying axial forces.

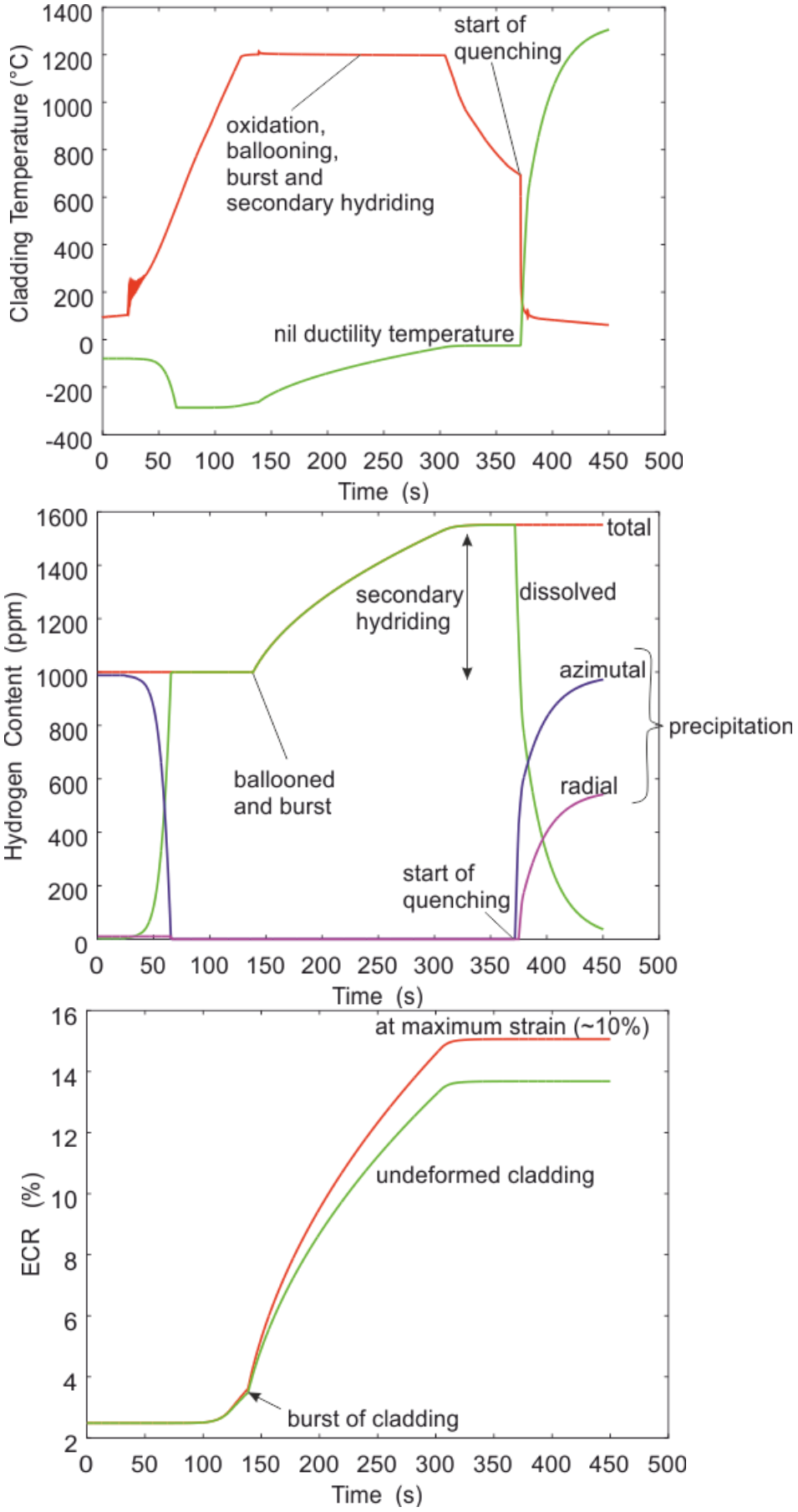

Fig. 7: Cladding temperature, hydrogen content and ECR evolution during the LOCA transient test.

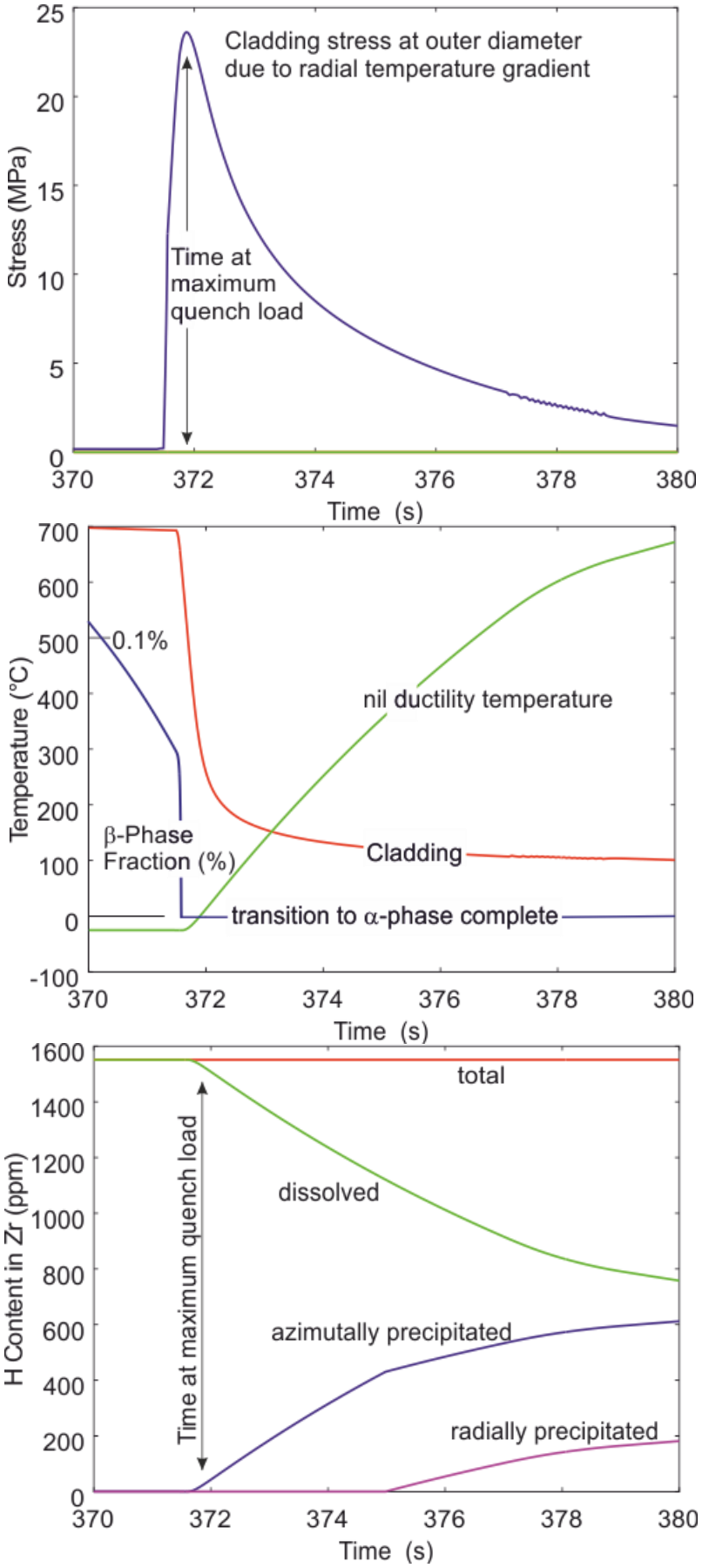

Fig. 8: Cladding stresses, temperature, β-phase fraction, hydrogen and hydride content of cladding during the cooldown.

The TESPA-ROD code simulation of the ITS test follows the cladding temperature as measured in the experiment (see Fig. 7). In accordance to the experiment, the code predicts oxidation, ballooning, burst and secondary hydriding. Figure 7 shows the TESPA-ROD code prediction for cladding temperature, hydrogen content and oxidation (ECR-%). The characteristic behaviour like enhanced oxidation and subsequent secondary hydriding occurs after burst of cladding at about 140 s of transient time.

With the oven shutdown, temperature decreases and α-β phase transformation begins. At start of quenching cladding temperature is fallen to 700 °C, where (according to the prediction of the TESPA-ROD's dynamic phase transition model) already 99.9 % fraction of the cladding returned to α-phase (see blue curve in mid-graph in Fig. 8).

At start of quench process the predicted oxidation is between 14 % and 15 % ECR, while the hydrogen content is at about 1600 ppm. The ECR limiting curve at this cladding condition is largely exceeded (compare with ECR curve in figure 2). Also the NRC limiting curve (the hydrogen content before secondary hydriding is about 1000 ppm) indicates for 14 % ECR and 1000 ppm H a none acceptable state of the cladding (compare with US.NRC curve in figure 2). In contrast to these limiting curves the Nagase and Fuketa ITS tests show for partially restrained cladding below 535 N axial force a none failure behaviour of the cladding at this cladding condition.

This remarkable test result indicates a failure threshold which is far from the nil-ductility line (limiting ECR curve with R=1) thus extremely large safety margins with regard to the limiting ECR curve are available. Although detrimental effects like oxidation, ballooning and secondary hydriding have taken place, the cladding withstands the subsequent thermal shock without breaking when the axial force is below 535 N. We presume there must be more ductility available than expected when considering both the ECR level and hydride content level.

Figure 8 puts a zoom on the time development from figure 7 during quench period. Additional to figure 7 the thermal load due to quenching has been plotted, which is deduced from the temperature gradient across the cladding according to equation (10) with $\sigma_{\Theta\Theta}$. This quench load reaches its maximum at about 372 s. But nil-ductility temperature occurs at about 373 s when the quench load maximum is already gone. Therefore, at the time of maximum quench load ductility is available although oxidation and hydriding are exceeding limiting curves.

This result suggests assessing claddings ductility on the basis of precipitated hydrides only instead of taking the entire hydrogen content in the cladding because precipitation has a significant time delay. This aspect is even more pronounced if one considers the quantity of radially precipitated hydrides only. There exists a further delay in precipitation of radial hydrides because the temperature gradient across the cladding thickness (thermal diffusion, Soret effect) promotes the precipitation of azimuthal hydrides (see Fig. 8 for H content in Zr). It is well-known that radial hydrides affect cladding's ductility only and azimuthal hydrides are of low importance for ductility.

6 Discussion and Conclusion

In the past, limiting ECR curve has been deduced via FEM technique from ring compression tests. This limiting curve (nil-ductility curve from equation (1) at R=1 and T=135 °C) involves paramount safety margins when judged on ITS tests of Nagase and Fuketa.

Although ITS tests even introduce penalizing axial stresses, these tests reveal that cladding's ductility during quenching is largely available, that is, ratio of burst stress to yield stress in ITS test is above unity (R>1). In contrast the evaluation of equation (1) for both measured quantity of oxidation (high ECR level) and measured quantity of pre-test hydrogen content suggests that this ratio would be below unity (R<1). Furthermore, taking into account secondary hydride uptake plus pre-test hydride content in equation (1) such ratio would be even more far below unity (R<<1).

It is presumed that among other effects the delay in hydrogen precipitation may largely explain this discrepancy between limiting curve (R=1) and ITS test data for cladding failure with high content of ECR and high content of hydrogen.

Therefore the TESPA-ROD code has been accomplished with a hydrogen precipitation model. This model is based on recent precipitation measurements performed by ANL. The ANL precipitation tests have been accomplished with synchrotron technique which allows in situ XRD measurements of precipitating hydrides during temperature variation. The TESPA-ROD code reproduces these precipitation test data with high confidence level.

We expect that the precipitation model deduced from these XRD measurements allow an application to fast cooldown transients like those under LOCA condition. The expectation is based upon the fact that growth rate of precipitating hydrides is limited by proton diffusion and this diffusion is linearly driven by hydride concentration gradients (Fick's Law).

Furthermore, the application of the precipitation model requires Zircaloy to be in α-phase, because hydride precipitation was measured for α-phase Zircaloy only. According to TESPA-ROD's dynamic phase transformation model for Zircaloy under slow cooldown from 1200 °C to 700 °C, the phase transformation to α-phase is (even for 1600 ppm hydrogen content and oxidation of 15 % ECR) to 99.9 % complete at 700 °C. Thus applicability of the hydrogen precipitation model to subsequent fast cooldown from 700 °C to 100 °C (quenching under atmospheric condition in ITS test) is given.

In a numerical study the TESPA-ROD code analyses the time development of the mechanical quench load as has been observed in the ITS test and compares this development with the development of the nil-ductility prediction. This kind of nil-ductility prediction supposes a shape of hydride precipitates as observed in RCTs. It is to be expected that the same shape of precipitates occur in ITS tests, because both tests (RCTs and ITS) are characterized by the same fast cooldown rate.

It turns out that the maximum of mechanical load occurs before the nil-ductility is reached. Therefore, much ductility is available at the time of maximum quench load although both oxidation level (e.g. ECR level up to 15 %) and hydrogen content (e.g. 1600 ppm) are far above the limiting curve.

This numerical study suggests not relying on the total content of hydrogen when assessing cladding's ductility. We conclude that it is much more realistic to account for precipitating hydrides only during quenching instead of the total hydride content. It also relativizes the necessity of predicting the secondary hydriding with high confidence.

References

[1] Nagase, F.; Fuketa, T.; "Effect of Pre-Hydriding on Thermal Shock Resistance of Zircaloy-4 Cladding under Simulated Loss-of-Coolant Accident Conditions", Integral Shock Tests, Journal of Nuclear Science and Technology, 41:7, 723-730, 2004

[2] Nagase, F.; Fuketa, T.; "Behavior of Pre-hydrided Zircaloy-4 Cladding under Simulated LOCA Conditions", Journal of Nuclear Science and Technology, Vol. 42, No. 2, p. 209–218, 2005

[3] Herb, J, Sievers, J, Sonnenburg, H-G; "A new cladding embrittlement criterion derived from ring compression tests", Nuclear Engineering and Design, Volume 273, p. 615-630, 2014

[4] Hache, G.; Chung, H. M.: "The History of LOCA Embrittlement Criteria, 28. Water Reactor Safety Information Meeting", Bethesda, MD, United States, NUREG/CP-0172, p. 205-237, 23-25 Oct 2001

[5] Stuckert, J. et al.; “Results of the refernce bundle test QUENCH-L1 with Zircaloy-4 claddings performed under LOCA conditions”, KIT Scientific reports 7651, ISSN 1869-9669, 2013

[6] U.S.-NRC, Office of Nuclear Regulatory Research: Draft Regulatory Guide DG-1263. ADAMS Accession No. ML12284A323. March 2014

[7] U.S. Department of Energy (DOE); “Three dimensional Fuel Pin Model Validation by Prediction of Hydrogen Distribution in Cladding and Comparison with Experiment”, Final Report DOE Nuclear Energy University Program (NEUP), Project No. 13-5180, 2018

[8] Lacroix, E. et al.; “Experimental determination of zirconium hydride precipitation and dissolution in zirconium alloy”, Journal of Nuclear Materials 509, 162-167, 2018

[9] Kearns, J.J.; “Terminal solubility and partitioning of hydrogen in the alpha phase of zirconium, Zircaloy-2 and Zircaloy-4”, Journal of Nuclear Materials, 22, Amsterdam, Netherlands, 1967

[10] McMinn, A. et al., “The Terminal Solid Solubility of Hydrogen in Zirconium Alloys”, Zirconium in the Nuclear Industry: Twelfth International Symposium, ASTM STP 1354, West Conshohocken, Pennsylvania, USA, 2000

[11] Une, K. et al., “The terminal solid solubility of hydrogen in irradiated Zircaloy-2 and microscopic modeling of hydride behavior”, Journal of Nuclear Materials, 389, Amsterdam, Netherlands, 2009

[12] Cinbiz et al.; “The effect of stress biaxiality on hydride reorientation threshold stress”, Penn State university, TopFuel 2015

[13] Foregon, T. et al.; "Experiment and Modeling of Advanced Fuel Rod Cladding Behaviour under LOCA Conditions: Alpha-Beta Phase Transformation Kinetics and EDGAR Methodology", 12th International Symposium, ASTM STP 1354, West Conshohocken, Pennsylvania, USA, 2000

[14] Baker, L.; Just, L.C.; Technical Report ANL-6548, Argonne National Laboratory, 1962.

[15] Cathcart, J.V. et al.; “Zirconium Metal-Water Oxidation Kinetics IV. Reaction Rate Studies”, ORNL/NUREG-17, 1977

[16] Sonnenburg, H.G.; Boldt, F.; Gesellschaft für Anlagen- und Reaktorsicherheit, Abschlussbericht GRS-464, 2017